

Bloch oscillations and quench dynamics of interacting bosons in an optical lattice

K. W. Mahmud,¹ L. Jiang,¹ E. Tiesinga,¹ and P. R. Johnson²

¹*Joint Quantum Institute, National Institute of Standards and Technology and University of Maryland, 100 Bureau Drive, Mail Stop 8423, Gaithersburg, Maryland 20899, USA and*

²*Department of Physics, American University, Washington, DC 20016, USA*

We study the dynamics of interacting superfluid bosons in a one dimensional vertical optical lattice after a sudden increase of the lattice potential depth. We show that this system can be exploited to investigate the effects of strong interactions on Bloch oscillations. We perform theoretical modelling of this system, identify experimental challenges and explore a new regime of Bloch oscillations characterized by interaction-induced matter-wave collapse and revivals which modify the Bloch oscillations dynamics. In addition, we study three dephasing mechanisms: effective three-body interactions, finite value of tunneling, and a background harmonic potential. We also find that the center of mass motion in the presence of finite tunneling goes through collapse and revivals, giving an example of quantum transport where interaction-induced revivals are important. We quantify the effects of residual harmonic trapping on the momentum distribution dynamics and show the occurrence of interaction-modified temporal Talbot effect. Finally, we analyze the prospects and challenges of exploiting Bloch oscillations of cold atoms in the strongly-interacting regime for precision measurement of the gravitational acceleration g .

PACS numbers: 03.75.Dg, 03.75.Lm, 67.85.-d, 91.10.Pp

I. INTRODUCTION

Ultracold atoms in optical lattices can simulate many of the phenomena associated with electrons in a periodic potential. Compared to real crystals, however, these artificial crystals made from laser light offer versatile control of system parameters such as the lattice depth, geometry and particle interactions [1]. Furthermore, long coherence times, absence of impurities, and low dissipation make them an ideal system to observe non-equilibrium quantum dynamics [2, 3]. One example is the observation of collapse and revival dynamics of bosonic matter wave coherence in a suddenly raised (*quenched*) optical lattice [4–6]. Another example is the observation of Bloch oscillations, periodic motion in momentum and real space, of ultracold atoms in an accelerating potential [7–9]. These two examples involve two different aspects of nonequilibrium dynamics: the single-particle physics of Bloch oscillations (BO) and the multi-particle physics of collapse and revival (CR) coherence oscillations which depend on atom-atom interactions [4, 10, 11].

Bloch oscillations arise when a constant force is applied to particles in a periodic potential [12]. They have been observed in many physical systems, including semiconductor superlattices [13] and ultracold atoms [7, 8, 14–16]. Bloch oscillations have also been used as a tool to explore band structures and their topological properties [17, 18], make precision measurements of gravity [15, 16, 19], and have been suggested as a probe to identify quantum phases [20, 21]. Although the single-particle physics of Bloch oscillations is well understood, there are still open questions regarding the role of particle-particle interactions [22–25].

In this paper, we perform a theoretical study of the dynamics of interacting ultracold bosons in a one-dimensional optical lattice whose axis is vertically aligned

with gravity. Transport in two horizontal directions is suppressed. This system, which has been explored in several recent experiments [4–6], is ideally suited for studying the interplay between particle-particle interactions and Bloch oscillations physics. We consider a quench scenario where, starting from an initial superfluid state, the lattice depth is suddenly increased so that tunneling is suppressed, the atom density frozen, and we are in the strong field regime $F \gg J$, where F and J are the gravitational potential energy difference and tunneling energy between two neighboring lattice sites, respectively. We show that the gravity-induced Bloch oscillations are strongly modified by interaction-induced matter-wave collapse and revivals.

In a deep lattice with negligible tunneling and higher-band excitation, the dynamics involves on-site phase evolution governed by the competing and independent effects of F and U , the two-body interaction energy. We study the dynamics in two limits – the strong- U ($U > F$) regime, and the strong- F ($F > U$) regime. Our analysis provides a unified theory for interacting BO which treats all regimes, and makes predictions that should be within reach of future experiments. Experiments in the strong- F regime have recently been performed by F. Meinert *et al.* [26].

We also investigate three dephasing mechanisms: (i) effective three-body interactions, (ii) finite value of tunneling, and (iii) residual harmonic trapping. In particular, we model in detail the momentum and real space oscillations of a lattice-trapped superfluid in the presence of both gravity and a background harmonic potential. We find that the dephasing effect due to effective three-body interactions becomes important for the strong- U regime. When $J \neq 0$, we predict that the Bloch oscillations of the center of mass of the atomic cloud should also go through collapse and revivals, demonstrating a novel interaction-

induced effect on quantum transport. We quantify how the presence of a harmonic trap during the dynamics quickly destroys coherence visibility, although we show that there can also be interaction-modified temporal Talbot revivals [27, 28].

We are also interested in the prospects for using Bloch oscillations of cold atoms for precision measurement of g . Most experiments have previously focused on the mean-field regime [15, 16, 19], where up to 20000 BO have been observed, although very recently experiments [26] have operated within the strongly-correlated, deep lattice regime. We present estimates for the bounds on the residual harmonic trapping and finite tunneling that should allow observations of up to 50000 Bloch oscillations.

Most previous studies of BO of ultracold atoms have used the Gross-Pitaevskii equation to model the mean-field regime when the number of particle per lattice site is on the order of hundreds or thousands [3, 14, 16]. In contrast, we use the Bose-Hubbard Hamiltonian, and time-evolving block decimation (TEBD) algorithm [29] for our numerical simulations, to model the dynamics when there are a few atoms per lattice site and particle correlations need to be properly accounted for. We also obtain analytical approximations in the limits of coherent states and the Thomas-Fermi regime. Bloch oscillations for interacting bosons in this regime have been studied by Kolovsky and collaborators [22, 30–34], and the transport properties of Mott insulators under a constant force [35–37] and superfluids in a Galileo ramp [38] have also been investigated. Our focus here is on regimes where matter-wave collapse and revivals due to interactions is important.

The article is organized as follows. In Sec. II we present our model, define observables, and describe our computational methods. In Sec. III, we briefly consider collapse and revivals dynamics in a mean-field theory when the initial state is a coherent state. In Sec. IV, we present our results for the Bloch oscillations of strongly-correlated interacting bosons in a vertical lattice. In Sec. V, we investigate dephasing from effective three-body interactions, finite tunneling and residual harmonic trapping. In Sec. VI, we analyze the prospects for precision measurement of gravity. Finally, we summarize our results in Sec. VII.

II. MODEL AND METHODS

A. System

We consider quasi-one dimensional bosons in the lowest band of a periodic or lattice potential with period d . We assume that the particles are tightly confined in the two transverse directions such that tunneling and transverse excitations are negligible. Under these assumptions the system is initially described by the Bose-Hubbard Hamil-

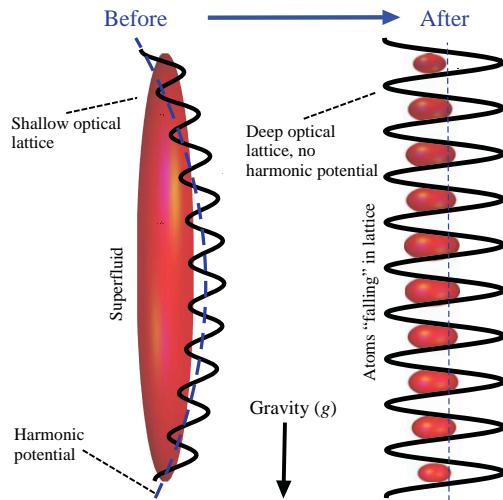


FIG. 1: (color online) Schematic of system. We start with a superfluid ground state in a shallow, vertically aligned optical lattice. A harmonic trap supports the atoms against gravity. The lattice depth is then suddenly increased and simultaneously the harmonic potential is turned off. These steps create a non-equilibrium state of atoms “falling” in the lattice under the influence of gravity and tunable atom-atom interactions.

tonian,

$$H_i = -J_i \sum_j (a_j^\dagger a_{j+1} + a_{j+1}^\dagger a_j) + \frac{U_i}{2} \sum_j n_j (n_j - 1) + V_{T,i} \sum_j j^2 \times n_j - F_i \sum_j j \times n_j, \quad (1)$$

where a_j^\dagger , a_j are boson creation and annihilation operators at lattice site j , $n_j = a_j^\dagger a_j$ is the boson number operator, J_i is the initial tunneling energy (hopping parameter) between nearest neighbors, and U_i is the initial on-site particle-particle interaction energy. In addition to the lattice potential, we include an external harmonic potential initially parameterized by energy $V_{T,i}$. The gravitational potential energy difference between neighboring lattice sites is $F_i = mgd$, where m is the atom mass, g is the acceleration of gravity, and $d = \lambda/2$ and λ is the wavelength of the laser that creates the periodic potential. For ^{87}Rb and a laser with $\lambda = 738$ nm, the gravitational energy is $F_i/h = 774$ Hz, where h is Planck’s constant. The tunneling energy J_i can be tuned by changing the lattice depth (typically $3E_R$ to $41E_R$, where $E_R = \hbar^2 k^2 / (2m)$ is the one-photon recoil energy, and $\hbar = h/(2\pi)$). The interaction energy U_i depends weakly on lattice depth, but can be tuned via a Feshbach resonance [39]. A magnetic field gradient can be applied to tune the value of F_i , as in [26].

We start with a superfluid ground state in a shallow, vertically aligned optical lattice (see Fig. 1). The atoms are initially supported against gravity by a harmonic potential. The linear potential of gravity shifts the minimum of the harmonic well, and there are no Bloch os-

cillations in the initial ground state. The depth of the optical lattice is then suddenly increased so that tunneling is suppressed. The parameter values before and after the quench are labelled by subscripts i and f , respectively. In the ideal quench scenario, tunneling is turned off ($J_i \rightarrow J_f = 0$), and simultaneously the harmonic trap is switched off ($V_{T,i} \rightarrow V_{T,f} = 0$, e.g., using the methods in [4]). The lattice ramp-up is assumed fast compared to atom-atom interactions, yet slow enough to prevent excitations to higher bands. The post-quench ideal final Hamiltonian is then

$$H_{\text{ideal}} = \frac{U_f}{2} \sum_j n_j (n_j - 1) - F_f \sum_j j \times n_j, \quad (2)$$

where U_f and F_f denote the interaction and gravitational energy parameters after the quench. These steps create a nonequilibrium state of the atoms “falling” in the lattice. In contrast, in Ref. [26] the system is “quenched” by suddenly changing $F_i \rightarrow F_f$ by changing an applied magnetic field gradient. Here we have taken $F_i = F_f = F$ throughout, since we focus on measuring g .

After a lattice hold time t_h , observables are measured either in-situ [40] or through time of flight imaging [4]. To see the effects of gravity on the atoms, imaging has to be done from the side as opposed to from the top or bottom.

We also model more realistic experimental conditions where there is residual harmonic trapping and finite tunneling. To find the ground states and simulate the time evolution, we use the time-evolving block decimation (TEBD) algorithm [29]. This is a near-exact numerical method where we can control the accuracy of our simulations. The TEBD algorithm is based on a matrix product state Ansatz and is equivalent to time-dependent density matrix renormalization group (DMRG) methods.

B. Observables

To analyze the non-equilibrium dynamics, we follow observables giving the center of mass position, momentum distribution, zero momentum occupation, and condensate fraction. The center of mass position x_{cm} (in units of d) is determined from density measurements as

$$x_{cm}(t) = \frac{1}{N} \sum_{j=1}^L j \langle n_j(t) \rangle, \quad (3)$$

where $N = \sum_j \langle n_j \rangle$ is total atom number and L is the total number of lattice sites.

The momentum distribution can be measured using time-of-flight expansion and is given by

$$\langle n_k \rangle = \frac{1}{L} \sum_{i,j} e^{ik(i-j)} g(i,j), \quad (4)$$

where $g(i,j) = \langle a_i^\dagger a_j \rangle$ is the single-particle density matrix (or Green’s function). As a special case, the occupation of the zero momentum mode is given by $\langle n_{k=0} \rangle =$

$(1/L) \sum_{i,j} g(i,j)$. For Bloch oscillations the momentum peak translates in k -space, and we define visibility as the occupation of the peak momentum denoted by $\langle n_{k,max} \rangle$.

Finally, we analyze the condensate fraction f_c , which is defined as the largest eigenvalue of the single-particle density matrix $g(i,j)$, divided by N . This is a measure of the presence of Bose-Einstein condensation in an interacting many-body system [41].

In our treatment of time dependence of observables, we normalize the momentum distribution with its maximum value at initial time and define, $\langle \tilde{n}_k \rangle = \langle n_k \rangle / \langle n_{k=0} \rangle_{t=0}$. Similarly, we normalize other observables with the corresponding initial values and define $\langle \tilde{n}_{k,max} \rangle$, $\langle \tilde{n}_{k=0} \rangle$ and \tilde{f}_c , to facilitate comparisons.

III. COHERENT STATE DYNAMICS

We can obtain analytic expressions for the collapse and revival dynamics if we assume that the initial superfluid is a product of coherent states $|\alpha_j\rangle$ in each site j . Such a state could be achieved experimentally if U_i is initially tuned to near zero. If a coherent state is suddenly projected (quenched) into a deep optical lattice, the resulting non-equilibrium state shows collapse and revival in coherence due to interactions, as first observed in Ref. [5].

The momentum distribution after the quench is then given by

$$\langle n_k(t) \rangle = \frac{1}{L} \left| \sum_j \langle a_j^\dagger(t) \rangle e^{-ijk} \right|^2 - \frac{1}{L} \sum_j |\langle a_j^\dagger(t) \rangle|^2 + \bar{n} \quad (5)$$

where $\bar{n} = N/L$ is the average atom occupation per site.

The Hamiltonian governing the post-quench dynamics when $J = 0$, is $H_f = H_{\text{ideal}} + V_{T,f} \sum_j j^2 n_j$, and the annihilation operator in the Heisenberg picture simplifies to

$$a_j(t) = e^{iH_f t/\hbar} a_j e^{-iH_f t/\hbar} = e^{-i(U_f n_j + V_{T,f} j^2 - F_j)t/\hbar} a_j \quad (6)$$

If we assume that the lattice is homogeneous and large, then $\langle a_j(t) \rangle = \alpha \exp[|\alpha|^2 (e^{-iU_f t/\hbar} - 1)] e^{i(-F_j + V_{T,f} j^2)t/\hbar}$. From here we can define the quantity,

$$v(t) = |\langle a(t) \rangle|^2 = \bar{n} e^{2\bar{n}[\cos(U_f t/\hbar) - 1]}, \quad (7)$$

where $\bar{n} = |\alpha|^2$ and the CR oscillation period is $T_U = h/U_f$.

When only the gravitational potential is present during the dynamics, the momentum distribution for a homogeneous system is given by,

$$\langle n_k(t) \rangle = \left(\frac{1}{L} \frac{\sin^2[(kd + \omega_B t)L/2]}{\sin^2[(kd + \omega_B t)/2]} - 1 \right) \times v(t) + \bar{n}. \quad (8)$$

where $\omega_B = F/\hbar$. A similar expression can be derived when the initial density $n_j = |\alpha_j|^2$ depends on position (e.g., for a Thomas-Fermi initial profile).

When only a harmonic trap is present during the evolution, we can obtain analytic expressions for the dynamics of $\langle n_{k=0} \rangle$ in two different approximations: (i) assuming a homogeneous pre-quench state, that is $n_j = \bar{n}$, and (ii) assuming a Thomas-Fermi initial density profile. For case (i), we obtain

$$\langle n_{k=0}(t) \rangle = \frac{1}{L} v(t) \left| \sum_j e^{iV_{T,f} j^2 t / \hbar} \right|^2 - v(t) + \bar{n}. \quad (9)$$

For case (ii), we use a Thomas-Fermi profile, $n_j = \bar{n}(1 - (V_{T,i}/\mu_0)j^2)$, where $\bar{n} = \mu_0/U_i$ and μ_0 is the chemical potential. Taking the continuum limit the sum turns into an integral, and after the change of variables $y = j\sqrt{V_{T,i}/\mu_0}$, we obtain

$$\langle n_{k=0}(t) \rangle = \bar{n} - v(t) + \frac{1}{L} v(t) e^{2\bar{n}} \times \left(\frac{\mu_0}{V_{T,i}} \right)^D \left| \int_{-b}^b y^{D-1} dy \sqrt{1-y^2} e^{(-\bar{n} + \frac{it\mu_0}{\hbar} \frac{V_{T,f}}{V_{T,i}})y^2} \right|^2. \quad (10)$$

Here D is the dimensionality of the system and $b = \frac{L}{2}\sqrt{V_{T,i}/\mu_0}$. We use Eqs. 9 and 10 in Sec. VI to model the early time decay of the zero momentum occupation, and analyze the effects of a residual harmonic trap on measuring g .

IV. DYNAMICS IN A VERTICAL LATTICE AND $J_f = 0$

In this section, we analyze the dynamics using a TEBD algorithm under idealized conditions where, after the quench, $J_f = 0$ (no tunneling) and $V_{T,f} = 0$ (no residual harmonic potential). We consider both strong- U ($U_f > F$) and strong- F ($F > U_f$) regimes.

Figure 2 shows the post-quench dynamics in the strong- U regime. For the initial superfluid, we choose $U_i/J_i = 3$ and lattice size $L = 32$. The initial atomic cloud, before the quench, is supported against gravity by a harmonic potential. We choose $V_{T,i} = 0.02U_i$ and $N = 40$. Unless otherwise noted, all figures will use these pre-quench values. To induce Bloch oscillations, the harmonic potential is turned off simultaneously with the lattice ramp. After the quench, we set $U_f = 5F$, which corresponds to $F = 774$ Hz and $U_f \approx 4$ kHz. The collapse and revival experiment of Ref. [4] would fall in this strong- U regime.

Figure 2(a) shows how the quasi-momentum distribution manifests two distinct behaviors. First, the peak or the center of the distribution moves uniformly in momentum space following $k(t) = k(0) + mgt/\hbar$; this results from the gravitational acceleration g . When it reaches the Brillouin zone boundary at $k = \pi$ it is Bragg scattered to $k = -\pi$. The motion continues and the peak returns to its original position at $k = 0$ in one BO period $T_B = h/F$. In this case of an infinitely deep lattice (i.e., $J_f = 0$), the atomic spatial density is frozen and the

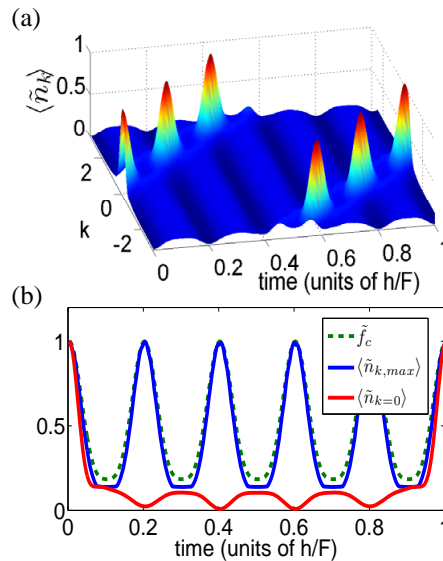


FIG. 2: (color online) Bloch oscillations collapse and revival dynamics in the strong- U regime when $U_f > F$. Here $U_f = 5F$. Shown are the dynamics of (a) the quasi-momentum distribution and (b) the peak momentum occupation and condensate fraction, as a function of hold time t_h in the lattice, given in units of h/F . Panel (a) shows that the atomic momentum performs two kinds of evolution: Bloch oscillations (BO) and collapse and revivals (CR) of coherence. The momentum peak travels in quasi-momentum space reaching the end of the Brillouin zone at $k = \pi$, reflecting to $k = -\pi$ and coming back to $k = 0$ to perform one Bloch oscillation with period h/F . During this time interval, the momentum peak also collapses and revives with period h/U_f . During collapse, atoms are distributed in quasi-momentum over the entire Brillouin zone. The observables in Panel (b) also reveal the simultaneous presence of BO and CR. Dynamics of condensate fraction \tilde{f}_c is not affected by the linear potential.

Bloch motion appears only in momentum space. The dynamics is driven by the relative gravitational phase shift $e^{imgdt/\hbar}$ between each neighboring sites.

Second, Fig. 2(a) shows that the momentum peak undergoes interaction-driven collapse and revival oscillations, with revival time T_U . In this example, there are five CR oscillations per BO, as $U_f/F = 5$. Here the BO and CR oscillations are decoupled; the analytic expression in Eq. (8) expresses this concisely. If $U_f = 0$ (no atom-atom interactions, which could be achieved experimentally via a Feshbach resonance), the momentum peak traverses the Brillouin zone with no CR oscillations. The role of interactions in BO in causing collapse and revivals is the same as the role interactions play in the CR experiments [4, 5].

CR oscillations can also be seen in a measurement of visibility by monitoring the momentum peak evolution $\langle \tilde{n}_{k,max} \rangle$ as depicted in Fig. 2 (b). We also plot the condensate fraction \tilde{f}_c and $\langle \tilde{n}_{k=0} \rangle$. The condensate fraction and visibility are closely related and proportional [45]. The condensate fraction dynamics shows

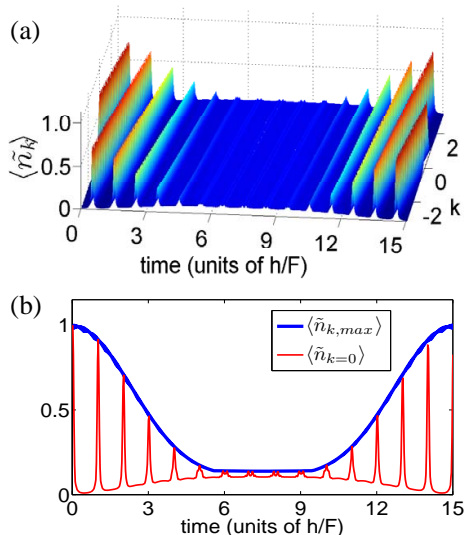


FIG. 3: (color online) Bloch oscillations collapse and revival dynamics in the strong- F regime when $F > U_f$. Here $F = 15U_f$. Panel (a) shows the quasi-momentum population $\langle \tilde{n}_k \rangle$ versus hold time. For this example, there is one CR cycle for every 15 BO. In this regime, $\langle n_{k=0} \rangle$ evolution, shown in Panel (b) reveals both CR and BO dynamics. The peak momentum evolution $\langle \tilde{n}_{k,max} \rangle$ shows only CR.

that the interaction-induced quantum depletion is decoupled from the evolution generated by the linear potential due to gravity or a uniform applied magnetic field.

Figure 3 shows post-quench dynamics in the strong- F regime, which could be achieved by using a Feshbach resonance to tune atom-atom interactions toward zero. The recent experiment [26] was performed in this regime. The initial superfluid corresponds to $U_i/J_i = 3$. After the quench we set $J_f = 0$ and $F/U_f = 15$. Figure 3(a) shows 15 Bloch oscillations in momentum space for every CR oscillation. Fig. 3(b) shows the dynamics of both the peak momentum occupation and zero momentum occupation, versus hold time. In this regime, collapse and revivals occur over many BO cycles. $\langle \tilde{n}_{k=0} \rangle$ evolution here reveals both CR and BO dynamics. CR can be viewed here as interaction-induced dephasing, and subsequent re-phasing, of the Bloch oscillations (see also [22]).

V. DEPHASING MECHANISMS

A. Effective 3-body interactions

In a deep lattice there are effective multi-body interactions due to collision induced virtual excitations to higher bands [11, 42, 43]. Quantum phase revival spectroscopy, based on the collapse and revival phenomenon, has been used to detect the presence of effective higher-body interactions [4, 6]. Here we examine the influence of effective three-body interactions on the Bloch oscillations CR dynamics. To model this physics, we add to the Hamil-

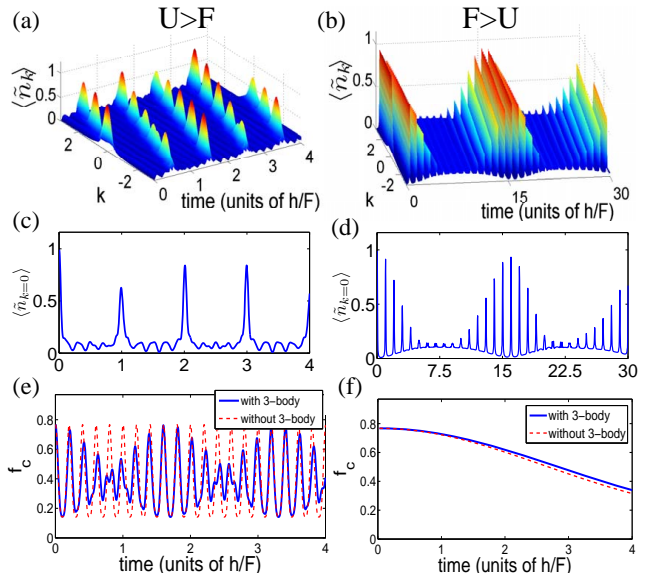


FIG. 4: (color online) Influence of effective 3-body interactions on the collapse and revivals of Bloch oscillation. Left column shows the strong- U limit of Fig. 2, and the right column shows the strong- F limit of Fig. 3. From top to bottom the panels show respectively $\langle \tilde{n}_k \rangle$, $\langle \tilde{n}_{k=0} \rangle$ and f_c . The three-body interaction strength is $U_3 = -0.12U_f$. The momentum distribution and BO dynamics is significantly modified during a single Bloch cycle for the strong- U regime. In contrast, the effect is far more gradual for the strong- F limit. This is highlighted in panels (e) and (f).

tonian in Eq. (2) the effective three-body term

$$H_{3B} = \frac{1}{3!} U_3 \sum_j n_j (n_j - 1) (n_j - 2) \quad (11)$$

where U_3 is the effective 3-body interaction energy.

Figure 4 shows the effects of three-body interactions in the strong- U (left column) and strong- F (right column) regimes for $U_f = 5F$ and $F = 15U_f$, respectively. In both cases we set $U_i/J_i = 3$ so that we consider the same initial state as in the previous section. Post-quench, we have $U_3 = -0.12U_f$ [42]. In Fig. 4 we plot the dynamics of three observables: the quasi-momentum distribution in the first Brillouin zone, the zero momentum occupation, and the condensate fraction (which is proportional to the visibility).

For the strong- U case in Fig. 4 (a) and (c), we see that the revival of the momentum peak after each BO cycle is incomplete, due to the presence of effective 3-body interactions. In contrast, in the strong- F regime shown in the right column of Fig. 4, the 3-body interactions lead to only a small modification of the oscillations, over the time interval shown. We quantify this in panels (e) and (f) by comparing f_c signals over the same time interval, with and without three-body interactions. The longer-period envelope in Panel (e) is due to effective three-body interactions and shows their significant influence in the strong- U regime. In Panel (f) the modification in the signal due to effective three-body interac-

tions is minimal on the same timescale. As expected, the influence of effective three-body interactions is far more prominent for the strong- U case. We note that the dephasing due to effective three-body interactions will also show revivals unless that timescale is longer than other dephasing mechanisms [4, 43].

B. Finite Tunneling

When there is finite tunneling $J_f \neq 0$ between lattice sites after the quench, Bloch oscillations manifest as position space oscillations as well as the momentum oscillations. We consider in this subsection finite- J_f still assuming the regime of $F \gg J_f$ and $V_{T,f} = 0$. Here

$$H_J = H_{\text{ideal}} - J_f \sum_j \left(a_j^\dagger a_{j+1} + a_{j+1}^\dagger a_j \right). \quad (12)$$

Figure 5 shows the effects of finite tunneling for both strong- U ($U_f/F = 5$ in top row) and strong- F regimes ($F/U_f = 15$ in bottom row). Panels (a) and (b) show the center-of-mass (COM) oscillations of the atomic density. Red and blue curves show cases with larger ($J_f = 0.1U_f$) and smaller tunneling ($J_f = 0.01U_f$), respectively. The influence of interactions can be seen in the COM motion. In Fig. 5(a), five small amplitude kinks are visible for every BO cycle, consistent with the parameter choice $U_f/F = 5$. In Fig. 5(b), the collapse and revival modulation occurs over 15 BO cycles, consistent with $F/U_f = 15$. We see in these simulations an example of interaction-induced collapse and revivals for real space quantum transport. We note that the spatial amplitude is less than a lattice spacing, for the parameter regimes explored here. The amplitude of the spatial oscillations is proportional to J_f , and depends on the competition of U_f and F .

Figures 5(c) and (d) show the BO dynamics of the quasi-momentum distribution for $J_f = 0.1U_f$. In the strong- U regime in Panel (c) we observe a rapid decay of the momentum peak caused by atoms tunneling to and interacting with atoms in neighboring sites [44]. Figures 5(e) and (f) show the dynamics of the condensate fraction f_c . In Panel (e), we see that the larger J_f value leads to the fastest damping of the condensate. For $J_f = 0.1U_f$ the BO signals in (c) and CR signals in (e) decay significantly within two BO periods. In contrast, the blue curve for small tunneling shows the expected interaction-driven CR oscillations, without significant decay of the revivals. For the strong- F regime in panels (d) and (f), we see that the decay is much slower over the same time span.

These simulations highlight how a combination of tunneling (J_f) and interactions (U_f) generates true damping. Finite- J_f allows tunneling to the neighboring sites and U_f causes interactions with atoms from neighboring sites which changes inter-site phase relationships, thus causing the overall decay of oscillations. In single-particle BO

physics with $U_f = 0$ and $F \gg J$, there is no damping. Similarly, in interacting BO physics with $J_f = 0$, there is no true damping as the oscillations revive on the two-body timescale U_f (and three-body time-scale U_3). It is the combination of J_f and U_f in the presence of F which causes dephasing. The presence of all three energy scales (J_f, U_f, F) causes the equally spaced Wannier-Stark ladders to split into a chaotic energy spectrum with multitude of avoided crossings. This has been identified in Refs. [22, 23, 30] as a reason for interaction-induced decoherence. The experiment reported in Ref. [26] explores this phenomenon.

C. Residual Harmonic Confinement

In the system described so far, the atoms are initially supported against gravity by a harmonic potential. To induce Bloch oscillations after the quench, we have assumed that the harmonic potential is turned off simultaneously with the lattice ramp, allowing the atoms to “fall” in the lattice. Alternatively, a sudden change in applied magnetic field (such that $F_f \neq F_i$) can be used to shift the location of potential minimum, as in [26]. The latter can be done with or without a change in the harmonic confinement. In either approach, in practice, there can remain a residual harmonic background $V_{T,f} \neq 0$.

In the CR experiments of Ref. [4], the harmonic potential was minimized using a combination of red and blue-detuned light. In Ref. [45], a theoretical analysis of CR in a harmonic trap was performed with an inhomogeneous Gutzwiller Ansatz formalism, showing rapid dephasing for a strong harmonic background. In the context of observing the Talbot effect with cold atoms [16, 27], harmonic confinement is a necessary ingredient. These experiments were analyzed using the Gross-Pitaevskii or discrete nonlinear Schrodinger equation (DNLSE) formalisms appropriate for the mean-field regime with many atoms [16, 27]. In this Section, we analyze, using the TEBD method, the effects of harmonic trapping both with and without a linear force in the strongly correlated regime.

1. Role of residual confinement without linear potential

First, we consider the effects of only residual harmonic confinement. This scenario can be achieved by suddenly quenching the superfluid without reducing the harmonic background. In Fig. 6, we show the dynamics assuming an initial state with $U_i/J_i = 3$. To differentiate the effects of the harmonic trap from interactions, we show in Figure 6(a) a density plot of the quasi-momentum distribution $\langle n_k \rangle$ setting $U_f = 0$. The figure shows initial dephasing from the harmonic confinement, with re-phasing (a full revival) after a period of $T_V = h/V_{T,f}$. There is also re-phasing in other quasi-momenta at intermediate times, which give an intricate, ordered structure called

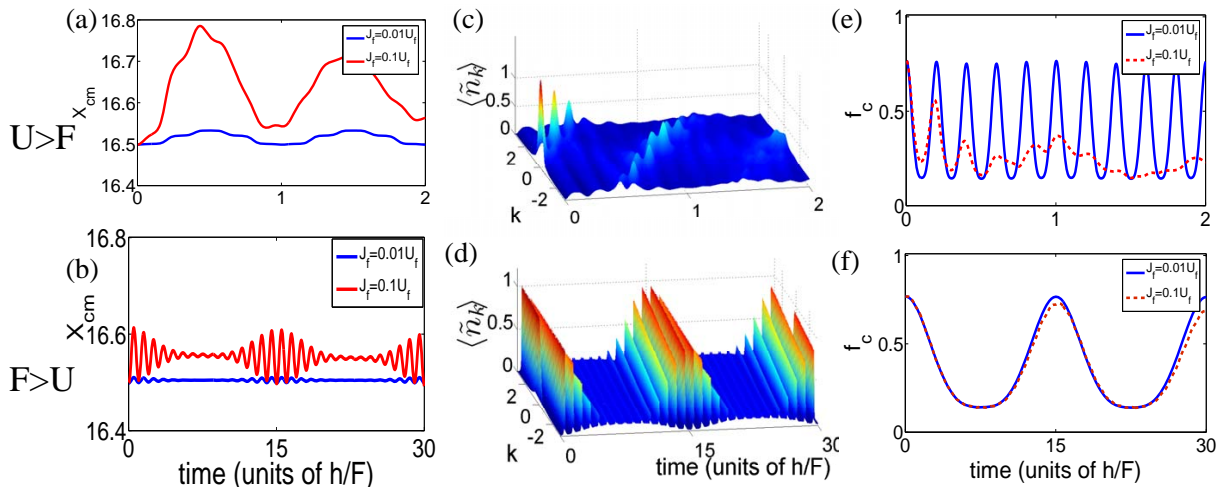


FIG. 5: (color online) Effect of finite tunneling on Bloch Oscillations revivals. Top and bottom rows show the strong- U and strong- F cases respectively. The center of mass (COM) oscillations shown in panels (a) and (b) have larger amplitudes for larger J_f , but they also damp at a faster rate. In Panel (b), we see that the COM performs CR oscillations, giving an example of quantum transport where real space collapse and revivals occur. Dynamics of momentum distribution for $J_f = 0.1U_f$ in panels (c) and (d), and condensate fraction in panels (e) and (f) show that higher values of J_f cause stronger decay in their signals. The competition among interactions (U_f), tunneling (J_f), and the linear potential (F) controls the complex dynamics.

a quantum carpet [46, 47]. Partial (fractional) revivals with two, three and integer n momentum peaks are seen at T_V/n , and there are further revivals symmetrically placed after $T_V/2$. The physics is analogous to the Talbot effect [28] familiar in optics, in which a coherent state experiencing multi-site diffraction gives rise to self-similar patterns in the near-field regime. The collapse and revivals in Fig. 6(a) have nothing to do with interactions, as $U_f = 0$, but are due to the quadratic phase relationship ($e^{iV_T j^2 t/\hbar}$) between the neighboring wells. Interestingly, the condensate fraction dynamics in Fig. 6(d) (blue line) shows that there is always a macroscopic occupation of a single quantum state, although the quasi-momentum has a fractal nature.

Figure 6(b) shows density plot of $\langle n_k \rangle$ when interaction is non-zero and stronger than the harmonic confinement energy scale ($U_f/V_{T,f} = 30$). This figure shows the combined effects of both the harmonic potential (with period $h/V_{T,f}$) and CR oscillations (with period h/U_f). For the parameter choice $U_f/V_{T,f} = 30$ there are 30 CR oscillations per harmonic period, as we can see in the condensate fraction dynamics in Panel (d). This plot also shows that condensate fraction dynamics is not affected by the external harmonic potential. This physics has been explained in Ref. [45]: the single particle density matrix of an inhomogeneous system is given by a unitary transformation of a homogeneous system, and consequently the eigenvalue time-evolution is the same in either a uniform or trapped system. The overall quantum-carpet pattern of quasi-momentum dynamics in Panel (a) is also seen in the strongly interacting case in Panel (b). However, the partial or fractional Talbot revivals that persist for the interacting case must be located at times when the interaction-revivals also occur; in this example that happens at factors of 30, i.e., at $t = 2, 3, 5, 6, 10$ in units of

h/U_f , and at symmetric times around the midpoint.

Additional insight can be obtained through analysis of the dynamics of the zero-momentum occupation shown in Fig. 6(c). The $k = 0$ population quickly decays and then revives after period $h/V_{T,f}$. The red curve ($U_f = 30V_{T,f}$) and the blue curve ($U_f = 0$) show that decay of the population, driven by the harmonic background, occurs irrespective of the value of U_f . Analyzing the early time dependence of the population decay yields information on the number of CR or BO cycles that can be readily observed in an experiment. In this example, the decay is so fast that only 3 CR oscillations can take place before harmonic dephasing dominates.

Finally, we note that there can be two other types of initial spatial shifts that have been neglected in our simulations. The first, trap shift, is due to the displacement of the center of the harmonic trap within a single lattice spacing. The second, cloud shift, is the displacement of the center of the atomic cloud from the center of the trap caused by gravitational sag. Trap shift has been found to influence the dynamics [45] introducing a linear shift in time in the momentum position in the first Brillouin zone. These effects can be easily scaled away.

2. Role of residual confinement including gravitation (or linear) potential

We now analyze the dynamics when the harmonic potential is only partially turned off during the quench, and there is a linear external potential present such that the location of the trap minimum suddenly shifts with the quench. We also include small but finite tunneling ($J_f \neq 0$). We expect the dynamics to simultaneously manifest gravity-driven BO, interaction-driven CR os-

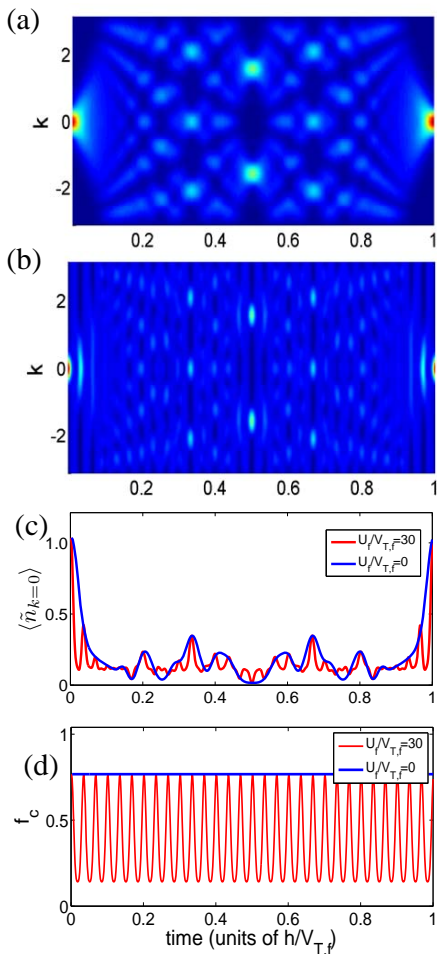


FIG. 6: (color online) Collapse and revivals dynamics in the presence of a harmonic trap. The quadratic term in the Hamiltonian due to the harmonic potential gives rise to a temporal Talbot effect familiar in optics. Panel (a) depicts a density plot of $\langle n_k \rangle$ for noninteracting ($U_f = 0$) system showing fractional momentum revivals. Panel (b) shows density plot of $\langle n_k \rangle$ for an interacting system where $U_f/V_{T,f} = 30$. The interactions destroy the Talbot revivals except at times that are integer multiples of h/U_f , i.e., at $t = 2, 3, 5, 6, 10$ in units of h/U_f , and at symmetric times around the midpoint. Lighter colors denote higher peaks in the momentum distribution while darker shades denote smaller populations. Panel (c) overlays the zero-momentum population for the above two cases. Panel (d) shows the condensate fraction f_c influenced only by the interactions. For $U_f = 0$, f_c is constant.

cillations, a harmonic-background-induced Talbot effect, and the effects of tunneling.

Figure 7(a) shows the quasi-momentum distribution versus hold time when $F = 0$ and $U_f = 2V_{T,f}$. We see the competing effects of the harmonic potential and interactions as described earlier, with the occurrence of fractional revivals. Figures 7(b), (c), and (d) show the dynamics versus hold time with $U_f = 2V_{T,f}$, $F = 60J_f$, and $F = 15U_f$ (the strong- F regime). The revivals in Panel (b) are strongly modified by the Bloch oscillations, which cause the momentum peaks to translate uniformly

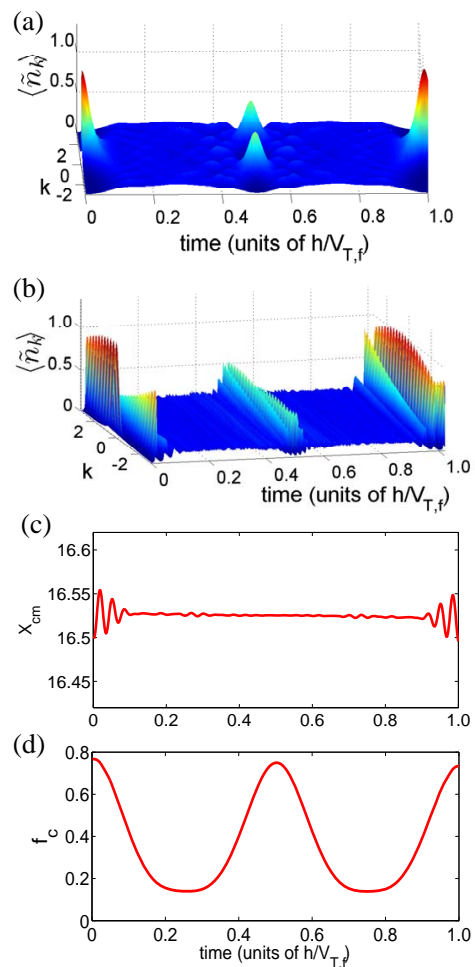


FIG. 7: (color online) Effect of harmonic trapping on Bloch oscillations revivals. The figure shows momentum distribution dynamics without [Panel (a)] and with [Panel (b)] the influence of a linear (e.g. gravitational) potential, respectively, and with $F = 15U_f$, $U_f = 2V_{T,f}$, and $J_f = U_f/4$. In Panel (b) the Talbot peaks seen in Panel (a) are moving in k -space due to Bloch oscillations. Panel (c) shows the center of mass motion, which contains signatures of interaction, the linear accelerating potential, the harmonic trap, and finite tunneling. Its Bloch oscillations goes through a CR sequence which is suppressed by harmonic trap Talbot revivals at $\frac{1}{2}h/V_{T,f}$. Panel (d) shows the condensate fraction f_c .

in k -space and reflect at the edge of the Brillouin zone. Figures 7(c) and (d) show dynamics of the center-of-mass and condensate fraction, respectively. The real space oscillations in Panel (c) contains signatures of all the competing terms – the fast modulations are due to BO, the collapse and revival of BO is due to interaction, and the suppression of interaction-induced revival at $\frac{1}{2}h/V_{T,f}$ is due to harmonic trap effects. The COM motion itself is due to finite tunneling, while the condensate fraction (f_c) dynamics in Panel (d) shows that CR oscillations are solely due to non-zero U_f , with slow decay due to tunneling-induced dephasing, but (again) no dependence on the harmonic confinement. Its dephasing is also unaf-

ected by gravity. In our treatment of BO in this paper, the example shown here may be most relevant to an actual experimental system since all of these effects will be present in practice, to some degree.

VI. MEASUREMENT OF g

Atomic Bloch oscillations have yielded a new method for making precision measurements of forces. Gravitational acceleration g has been measured with different degrees of precision with atomic BECs and thermal atoms in a vertical optical lattice [14–16, 19, 48]. Different aspects of Bloch oscillations physics have been used for attaining high precisions – for example, Ref. [15] used lattice modulation at the 5th harmonic of the Bloch frequency to induce tunneling, and Ref. [16] used a Feshbach resonance to turn off interactions to reduce interaction-induced dephasing due to mean-field nonlinearity. We investigate here the prospects and challenges for the precision measurement of g within a system of strongly interacting bosons in a suddenly quenched vertical optical lattice.

The precision of the measurement of g in a Bloch Oscillations experiment depends on the number of BO cycles that can be observed. Another factor is the narrowness of the momentum distribution for the initial and the time-evolved state. In the experiments of [15, 16], performed in the GP regime, they were able to follow the dynamics for 10 s to 20 s and observe approximately 20000 BO cycles. On the other hand, experiments on CR [4] followed the dynamics for 20 ms, long enough time for 20 to 30 BO cycles. Reasons for the fast decay of signals in the CR experiments could include: pumping energy into the system due to the quench, presence of a residual harmonic trap, presence of finite tunneling, three-body loss and other interaction related losses, and the effect of changing of the Wannier function [49]. Here we analyze the effects of a harmonic trap and finite tunneling, and calculate bounds on their values for observing up to 50000 BO cycles.

A. Bounds on residual harmonic trap

We have shown in Sec. V that the presence of a residual harmonic trap during the dynamics causes rapid decay in $\langle n_k \rangle$. In separate experiments involving BO [27] and CR [4], harmonic trap effects were minimized; however, a number was not given on how small the value is. Even a minute trap strength can have a significant effect over many oscillations. Figure 8(a) shows a TEBD simulation of the early time decay of $\langle \tilde{n}_{k=0} \rangle$ with $V_{T,f}/F = 0.002$, for $F = 2$, $U_f = 10$ and $L = 32$, when the initial state is homogeneous $V_{T,i} = 0$ and final tunneling is suppressed $J_f = 0$. We see that Bloch and CR oscillations occur on timescales h/F and h/U_f respectively, and they decay due to the residual harmonic trap, following a common

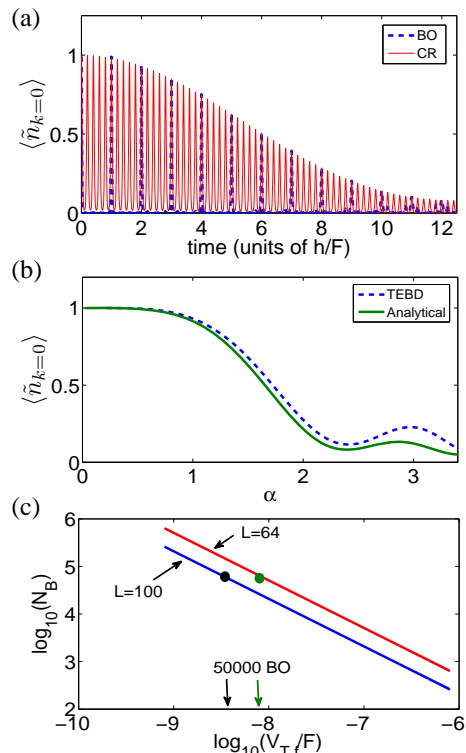


FIG. 8: (color online) Bounds on the number of Bloch oscillations due to a residual harmonic trap. Panel (a) depicts a TEBD simulation with $L = 32$ of the effects of a trap for $V_{T,f} = 0.002F$, $F = 2$, and $U_f = 10$. We see that both the Bloch (dotted line) and CR (full line) oscillations with period h/F and h/U_f are modified by a decay envelope characteristic of the trap strength. Here we show only the short time dynamics where the trap-induced decay of visibility takes place. In Panel (b), we show the analytical envelope of $\langle \tilde{n}_{k=0} \rangle$, Eq. (13), assuming that the initial superfluid state is a coherent state and homogeneous, as a function of scaled time $\alpha = L\sqrt{V_{T,f}t_h}/(2\hbar)$. We compare this to TEBD results with $L = 32$ showing a good match for the initial decay. Panel (c) shows a $\log\text{-}\log$ plot of the number of BO cycles when $\langle \tilde{n}_{k=0} \rangle$ drops to $1/e$ of its initial value, as a function of residual harmonic trap strengths for lattice sizes $L = 64$ (red curve) and 100 (blue curve). The dots and arrows on the $V_{T,f}/F$ -axis denote the corresponding bound for 50000 BO.

envelope function. The envelope function can be understood from the approximate continuum form of Eq. (9) assuming an initial superfluid that is homogeneous and coherent, evolving in a harmonic trap of strength $V_{T,f}$. The effects of $V_{T,f}$, U_f and F are separable and the initial decay of the envelope function, is given by the analytical expression

$$\langle n_{k=0}^{env}(t_h) \rangle \approx \pi \frac{|\text{erf}(ie^{i\pi/4}\alpha)|^2}{4\alpha^2} \quad (13)$$

where erf is the error function, $\alpha = L\sqrt{V_{T,f}t_h}/(2\hbar)$, L is the number of lattice sites and t_h is the hold time. Figure 8(b) shows $\langle n_{k=0}^{env} \rangle$ as a function of the dimensionless variable α . The expression is universal for any harmonic trap and lattice size; decay for different trap

strengths can be scaled to fall on this same curve. A comparison of analytical result with TEBD simulations, which include correlations due to tunneling in the initial superfluid, shows a good match for the initial decay.

Using Eq. (13) we find that we can quantify the number of BO, N_B , that can be observed by the hold time when the envelope of $\langle \tilde{n}_{k=0}(t) \rangle$ decays to $1/e$ of its initial value. This gives a relationship between the background trap strength ($V_{T,f}/F$) and N_B ,

$$N_B \approx \frac{1}{2\pi} \frac{e^2 \sqrt{\pi}}{L^2} \frac{F}{V_{T,f}} \quad (14)$$

In Fig. 8(c) we plot the value of $V_{T,f}/F$ needed to observe N_B Bloch oscillations for lattice sizes $L = 64$ and 100 ; note that it is a *log-log* plot. The filled circles represent the point for 50000 BO and the arrows below indicate the trap strengths required. For the experimentally relevant lattice sizes between $L = 50$ and 100 , the trap strength needs to be extremely small, e.g., $V_{T,f}/F \approx 10^{-8}$, to observe BO cycles beyond the current maximum value of 20000 [27]. Larger lattice sizes make the constraint more severe.

If the initial pre-quench state is trapped, it causes density inhomogeneity and N_B increases up to 20%. Then N_B depends on a combination of initial trap, total atom number and the density profile, and specific cases must be analyzed numerically. We note that the momentum width for an initially trapped case is bigger, and it spreads more quickly during the dynamics, eventually making the number of observable BO smaller. The overall effect of an initial trap is not significant compared to that of the residual trap, and hence our analysis here using an initially homogeneous density profile gives a good approximation for the bounds on $V_{T,f}$.

B. Bounds on finite-J effects

In an ideal BO collapse and revival scenario $J_f = 0$ and the momentum peak revives completely. For $J_f \neq 0$, Fig. 5 showed that CR oscillation amplitudes slowly decay, and similarly the BO signal dephases due to the competition among J_f, U_f and F . Here we analyze the bounds on the number of Bloch oscillations for a finite non-zero value of J_f/U_f and J_f/F . For this, we assume that J_f is small: $F \gg J_f$ and $U_f \gg J_f$.

In Fig. 9 we analyze the decay of CR oscillations of $\langle \tilde{n}_{k=0} \rangle$ for different values of J_f/U_f and $F = 0, V_{T,f} = 0$, using TEBD numerical simulations. The initial superfluid state is a homogeneous coherent state with $U_i/J_i = 0, \bar{n} \approx 1.5$ and $L = 32$. Figure 9(a) shows the dynamics in units of interaction timescale h/U_f where the expected higher rate of decay for larger tunneling values is evident. If the same data is plotted in units of h/J_f , as shown in Panel (b), a common envelope function is seen to characterize the decay of $\langle \tilde{n}_{k=0} \rangle$. This implies that for a specific value of tunneling J_f/U_f , the signal decay after one oscillation is equal to that of the M th oscillation for the

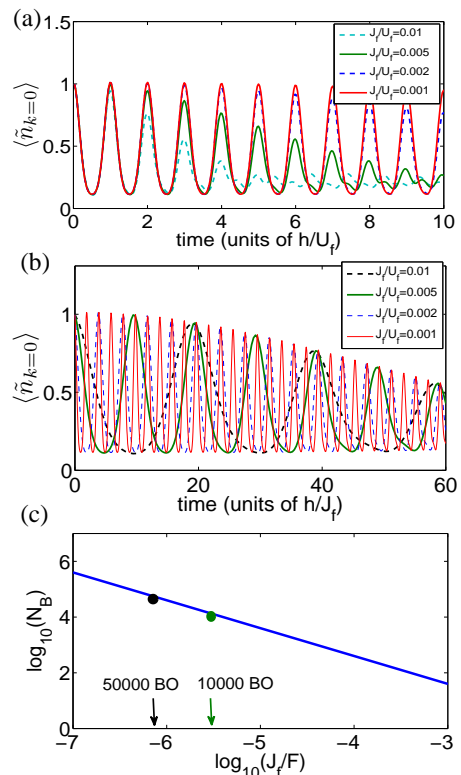


FIG. 9: (color online) Bounds on the number of Bloch oscillations due to finite- J_f . Panel (a) depicts the $\langle \tilde{n}_{k=0} \rangle$ collapse and revival signal decay for different values of J_f/U_f , as a function of hold time, in units of interaction time-scale h/U_f . The homogeneous initial superfluid state has $U_i/J_i = 0$ and $\bar{n} = 1.5$. As J_f/U_f increases, the number of observable oscillations decrease as expected. The revivals occur approximately at integer multiples of h/U_f , deviating slightly for increasing J_f/U_f . In (b) we plot the same data as in (a), but in units of tunneling time h/J_f . We see that the damping of the signals can be described by a common envelope function. Finding the decay for one value of J_f/U_f , we can find the damping of M th-oscillation by a simple scaling. Panel (c) shows the number of observable Bloch oscillations N_B for different values of J_f/F ; to observe 50000 BO, $J_f/F \approx 0.8 \times 10^{-6}$.

smaller value $\frac{1}{M} J_f/U_f$. The reference J_f/U_f needs to be small for this relationship to hold. For values considered in Fig. 9(b), this holds true. The damping of the first oscillation revival analyzed in Refs. [50, 51] is consistent with our findings. We show here that this analysis can be extended to the M th oscillation, and propose a method to estimate the number of observable oscillations for smaller tunneling rate by calculating the oscillation decay for a larger one.

We can also make a connection with the number of observable BO, again defined by the time at which the envelope of $\langle \tilde{n}_{k=0} \rangle$ reaches $1/e$ of its initial value. In the presence of finite- J , the CR oscillations due to U_f and BO due to F are coupled as discussed in Sec. V.B. In the regime of interest, when $F \gg J_f$ and $U_f \gg J_f$, the effects of U_f and F on the oscillations are approximately separable. Figure 9(c) depicts the Bloch oscillations N_B

that can be observed for different values of J_f/F . To observe 50000 BO cycles, J_f/F value needs to be 0.8×10^{-6} .

The value of J_f depends on optical lattice depth V in the following way: $\frac{J_f}{U_f} = \frac{2\sqrt{2}d}{\pi a_s} e^{-2\sqrt{V}}$, where V is given in units of recoil energy E_r , a_s is the s-wave scattering length, and d is lattice spacing. We estimate that quenching to $V > 20E_r$ puts us into a regime of $J_f/U_f > 10^{-6}$ and depending on the ratio of F and U_f , $J_f/F > 10^{-6}$ can be achieved.

The damping of BO due to finite- J depends on several things: the initial average occupation, J_i/U_i , initial trap $V_{T,i}$ and force F , in addition to its dependence on J_f/U_f . We find here that knowing all the other parameters, the bounds on J_f/F and J_f/U_f to observe N_B oscillations has a linear dependence. We have not discussed even longer term behavior of the decay as the question of thermalization and equilibration can become important [52, 53]. The value of J_f/U_f should be small in precision measurement experiments such that a large number of Bloch oscillations can be observed before equilibration takes place.

VII. CONCLUSION AND SUMMARY

In this paper, we have shown that the effect of multi-particle interactions on Bloch oscillations physics is described by the physics of matter-wave revivals – full revivals for a decoupled lattice and partial revivals for a coupled lattice, all occurring on the interaction timescale. We performed a theoretical analysis of interacting ultracold bosons in a suddenly ramped one-dimensional optical lattice that is vertically aligned. This set up can be systematically tuned and exploited to study the effects of interactions on BO. We used the Bose-Hubbard Hamiltonian to model the dynamics in the strongly interacting regime, and studied the dynamics in two limits – the strong- U ($U > F$) regime, and the strong- F ($F > U$) regime, where U and F are respectively atom-atom interaction and linear potential strength, after the quench. We have used the time-evolving block decimation (TEBD) algorithm for our numerical simulations.

We analyzed three dephasing mechanisms for the oscillations – effective three-body interactions, finite value

of tunneling J and residual harmonic trapping. We find that the dephasing effect due to effective three-body interactions becomes important for the strong- U regime. When $J \neq 0$, we predict that Bloch oscillations of the center of mass of the atomic cloud should also go through collapse and revival modulations, demonstrating an example of quantum transport where real-space revivals occur. We also show that the presence of a harmonic trap during the dynamics quickly destroys coherence visibility of the atoms and gives rise to a temporal Talbot effect [27, 28], which survives in the strongly interacting few-atom regime. We further model in detail the momentum and real space oscillations of a lattice-trapped superfluid in the presence of gravity, a residual harmonic potential and finite tunneling.

In addition to studying the interplay between interactions and Bloch oscillations physics, we examine the prospects of measuring the gravitational acceleration g with high precision using a system of strongly-correlated ultracold atoms in a deep lattice. We present numerical and analytical results for error bounds on the residual harmonic trap and finite tunneling to go beyond the current maximum observation of 20000 Bloch oscillations. The analysis and characterization of a realistic experimental setup is a necessary step towards the goal of surpassing the current precision limit of g .

The ideas investigated here are extremely relevant in the light of current experimental efforts [26]. Further insights can be gained by studying more comprehensively the competition of F , U and J . Realistic conditions such as finite temperature and higher-band effects may also be relevant for cold atom experiments. The effects of interactions on Bloch oscillations in cold atoms and other systems deserve additional analysis for the exploration of fundamental physics as well as measurement applications.

Acknowledgments

We acknowledge support from the US Army Research Office under Contract No. 60661PH and the National Science Foundation Physics Frontier Center located at the Joint Quantum Institute.

-
- [1] I. Bloch, J. Dalibard, and W. Zwerger, *Rev. Mod. Phys.* **80**, 885-964 (2008).
 - [2] A. Polkovnikov, K. Sengupta, A. Silva, and M. Vengalattore, *Rev. Mod. Phys.* **83**, 863 (2011); J. Dziarmaga, *Adv. Phys.* **59**, 1063 (2010).
 - [3] O. Morsch and M. Oberthaler, *Rev. Mod. Phys.* **78**, 179 (2006).
 - [4] S. Will, T. Best, U. Schneider, L. Hackermüller, D.-S. Lühmann, and I. Bloch, *Nature* **465**, 197 (2010).
 - [5] M. Greiner, O. Mandel, T. W. Hänsch and I. Bloch, *Nature* **415**, 51 (2002).
 - [6] S. Will, T. Best, S. Braun, U. Schneider, and I. Bloch, *Phys. Rev. Lett.* **106**, 115305 (2011).
 - [7] M. B. Dahan, E. Peik, J. Reichel, Y. Castin, and C. Salomon *Phys. Rev. Lett.* **76**, 4508 (1996).
 - [8] S. R. Wilkinson, C. F. Bharucha, K. W. Madison, Qian Niu, and M. G. Raizen, *Phys. Rev. Lett.* **76**, 4512 (1996).
 - [9] M. G. Raizen, C. Salomon, and Q. Niu, *Phys. Today* **50**, No. 8, 30 (1997).
 - [10] E. Tiesinga and P. R. Johnson, *Phys. Rev. A* **83**, 063609

- (2011).
- [11] K. W. Mahmud and E. Tiesinga, *Phys. Rev. A* **88**, 023602 (2013).
- [12] F. Bloch, *Z. Phys.* **52**, 555 (1928); C. Zener, *Proc. R. Soc., London* **A145**, 523 (1934).
- [13] J. Feldmann, K. Leo, J. Shah, D. A. B. Miller, J. E. Cunningham, T. Meier, G. von Plessen, A. Schulze, P. Thomas, and S. Schmitt-Rink, *Phys. Rev. B* **46**, 7252 (1992).
- [14] B. P. Anderson and M. A. Kasevich, *Science* **282**, 1686 (1998).
- [15] N. Poli, F.-Y. Wang, M. G. Tarallo, A. Alberti, M. Prevedelli, and G. M. Tino, *Phys. Rev. Lett.* **106**, 038501 (2011).
- [16] M. Gustavsson, E. Haller, M. J. Mark, J. G. Danzl, G. Rojas-Kopeinig, and H.-C. Nägerl, *Phys. Rev. Lett.* **100**, 080404 (2008).
- [17] M. Atala, M. Aidelsburger, J. T. Barreiro, D. Abanin, T. Kitagawa, E. Demler, and I. Bloch, e-print arXiv:1212.0572 (2012).
- [18] L. Tarruell, D. Greif, T. Uehlinger, G. Jotzu, and T. Esslinger, *Nature* **483**, 302 (2012).
- [19] M. G. Tarallo, A. Alberti, N. Poli, M. L. Chiofalo, F.-Y. Wang, and G. M. Tino, *Phys. Rev. A* **86**, 033615 (2012).
- [20] A. V. Gorshkov, S. R. Manmana, G. Chen, J. Ye, E. Demler, M. D. Lukin, and A. M. Rey, *Phys. Rev. Lett.* **107**, 115301 (2011).
- [21] J. Carrasquilla, S. R. Manmana and M. Rigol, *Phys. Rev. A* **87**, 043606 (2013).
- [22] A. R. Kolovsky, *Phys. Rev. Lett.* **90**, 213002 (2003).
- [23] A. Buchleitner and A. R. Kolovsky, *Phys. Rev. Lett.* **91**, 253002 (2003).
- [24] G. Corrielli, A. Crespi, G. D. Valle, S. Longhi, and R. Osellame, *Nat. Comm.* **4**, 1555 (2013).
- [25] R. Khomeriki, D. O. Krimer, M. Haque, and S. Flach, *Phys. Rev. A* **81**, 065601 (2010).
- [26] F. Meinert, M. J. Mark, E. Kirilov, K. Lauber, P. Weinmann, M. Grobner, and H.-C. Nägerl, e-print arXiv:1309.4045 (2013).
- [27] M. Gustavsson, E. Haller, M. J. Mark, J. G. Danzl, R. Hart, A. J. Daley, and H.-C. Nägerl, *New J. Phys.* **12**, 065029 (2010).
- [28] M. S. Chapman, C. R. Ekstrom, T. D. Hammond, J. Schmiedmayer, B. E. Tannian, S. Wehinger, and D. E. Pritchard, *Phys. Rev. A* **51**, R14 (1995).
- [29] G. Vidal, *Phys. Rev. Lett.* **91**, 147902 (2003); **93**, 040502 (2004).
- [30] A. R. Kolovsky, *Phys. Rev. A* **70**, 015604 (2004).
- [31] A. R. Kolovsky, *Eur. Phys. J. Special Topics* **151**, 103-112 (2007).
- [32] A. R. Kolovsky and H. J. Korsch, *Int. J. Mod. Phys.* **18**, No.9 1235 (2004).
- [33] A. R. Kolovsky, H. J. Korsch and E. M. Graefe, *Phys. Rev. A* **80**, 023617 (2009).
- [34] D. Witthaut, M. Werder, S. Mossmann, and H. J. Korsch, *Phys. Rev. E* **71**, 036625 (2005).
- [35] S. Sachdev, K. Sengupta and S. M. Girvin, *Phys. Rev. B* **66**, 75128 (2002).
- [36] J. Simon, W. S. Bakr, R. Ma, M. E. Tai, P. M. Preiss, and M. Greiner, *Nature* **472**, 307 (2011).
- [37] C. P. Rubbo, S. R. Manmana, B. M. Peden, M. J. Holland, and A. M. Rey, *Phys. Rev. A* **84**, 033638 (2011).
- [38] M. Collura, H. Aufderheide, G. Roux, and D. Karevski, *Phys. Rev. A* **86**, 013615 (2012).
- [39] C. Chin, R. Grimm, P. Julienne, and E. Tiesinga *Rev. Mod. Phys.* **82**, 1225 (2010).
- [40] W. S. Bakr, J. I. Gillen, A. Peng, S. Foelling, and M. Greiner, *Nature* **462**, 74 (2009).
- [41] O. Penrose and L. Onsager, *Phys. Rev.* **104**, 576 (1956).
- [42] P. R. Johnson, E. Tiesinga, J. V. Porto, and C. J. Williams, *New J. Phys.* **11**, 093022 (2009).
- [43] P. R. Johnson, D. Blume, X. Y. Yin, W. F. Flynn, and E. Tiesinga, *New J. Phys.* **14**, 053037 (2012).
- [44] J. Schachenmayer, A. J. Daley, and P. Zoller, *Phys. Rev. A* **83**, 043614 (2011).
- [45] M. Buchhold, U. Bissbort, S. Will, and W. Hofstetter, *Phys. Rev. A* **84**, 023631 (2011).
- [46] A. R. Kolovsky, E. A. Gomez and H. J. Korsch, *Phys. Rev. A* **81**, 025603 (2010).
- [47] M. J. Mark, E. Haller, J. G. Danzl, K. Lauber, M. Gustavsson, and H.-C. Nägerl, *New J. Phys.* **13**, 085008 (2011).
- [48] F. Sorrentino, A. Bertoldi, Q. Bodart, L. Cacciapuoti, M. de Angelis, Y.-H. Lien, M. Prevedelli, G. Rosi, and G. M. Tino, *App. Phys. Lett.* **101**, 114106 (2012).
- [49] M. Lacki and J. Zakrzewski, *Phys. Rev. Lett.* **110**, 065301 (2013).
- [50] U. R. Fischer and R. Schutzhold, *Phys. Rev. A* **78**, 061603(R) (2008).
- [51] F. A. Wolf, I. Hen, and M. Rigol, *Phys. Rev. A* **82**, 043601 (2010).
- [52] T. Kinoshita, T. Wenger, and D. S. Weiss, *Nature* **440**, 900 (2006).
- [53] M. Rigol, V. Dunjko, and M. Olshanii, *Nature* **452**, 854 (2008).